



Apportioning Light Absorption of Ambient Aerosols to Black Carbon, Brown Carbon, and Lensing Effect Using a PAX-ISS Hybrid Method: Insights into Absorption Enhancement

Yi Shen^{1,2}, Guorui Zhi^{1*}, Wenjing Jin¹, Yao Kong³, Yuzhe Zhang^{1*}, Zhengying Li⁴, Jianzhong Sun⁵, Yuankai Wang¹, Zhijian Liang¹

¹State Key Laboratory of Environmental Criteria and Risk Assessment, Chinese Research Academy of Environmental Sciences, Beijing 100012, China

²Department of Atmospheric Science & School of Earth Science, Yunnan University, Kunming 650500, China

³Dongying Meteorological Bureau, Dongying 257091, China

⁴Beijing Municipal Ecological and Environmental Monitoring Center, Beijing 100048, China

⁵School of Physical Education, Chizhou University, Chizhou 247000, China.

*Correspondence: Guorui Zhi (zhigr@craes.org.cn) and Yuzhe Zhang (yzzhang943@foxmail.com)

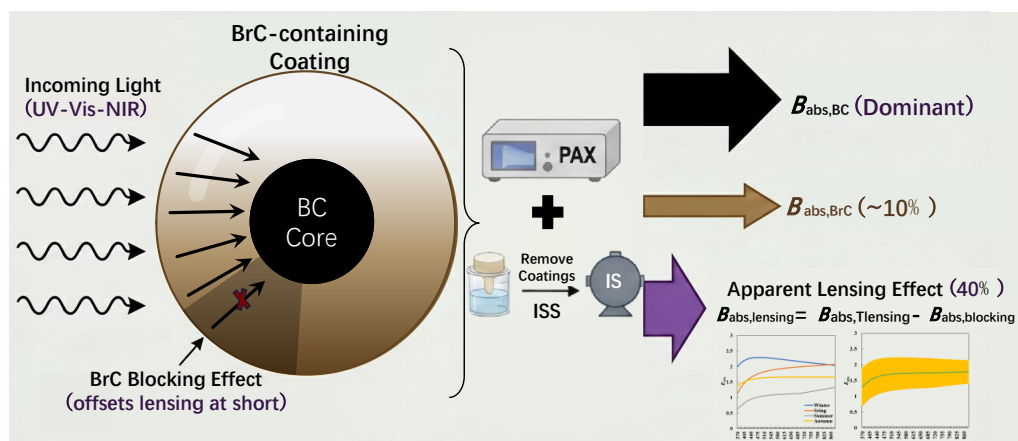


1 **Abstract**

2 Accurately apportioning aerosol light absorption to black carbon (BC), brown carbon
3 (BrC), and the lensing effect is crucial for constraining aerosol radiative forcing, yet
4 existing methods often fail to resolve all three components simultaneously. Here, we
5 introduce and demonstrate an integrated measurement framework that couples
6 photoacoustic spectroscopy (PAX) with an integrating sphere system using solvent
7 mediation (ISS). This PAX-ISS hybrid method quantifies the total absorption of
8 ambient aerosols ($B_{\text{abs,coated}}$) and removes the lensing effect via solvent-mediated
9 coating removal to obtain the lensing-free absorption ($B_{\text{abs,uncoated}}$). The absorption
10 solely due to the lensing effect ($B_{\text{abs,lensing}}$) is then directly quantified as their difference:
11 $B_{\text{abs,lensing}} = B_{\text{abs,coated}} - B_{\text{abs,uncoated}}$. The lensing-free absorption ($B_{\text{abs,uncoated}}$) is further
12 spectrally decomposed into BC and BrC contributions ($B_{\text{abs,BC}}$ and $B_{\text{abs,BrC}}$) using a dual-
13 wavelength iterative algorithm. Applied to seasonal samples in Beijing during 2023, the
14 method revealed that BC dominated light absorption, with BrC contributing
15 approximately 10% annually. The apparent lensing-induced enhancement averaged 40%
16 of total absorption but exhibited strong seasonal (4.6–52.0%) and spectral variations,
17 contracting sharply at shorter wavelengths—a pattern indicative of a BrC “blocking
18 effect” that offsets lensing enhancement. Our field measurements provide, for the first
19 time, direct observational evidence supporting this blocking effect, which was initially
20 proposed by other researchers based solely on numerical simulations. The annual
21 wavelength-averaged absorption enhancement factor (E_{abs}) was 1.69 ± 0.10 . This
22 methodology provides a robust, observationally constrained approach to apportion
23 aerosol absorption, offering refined insights for climate modeling.



24 Graphical Abstract



25



26 **1 Introduction**

27 Black carbon (BC) and brown carbon (BrC) are critical components of atmospheric
28 particulate matter due to their strong absorption of solar radiation (Laskin et al., 2025;
29 Xie et al., 2025; Yang et al., 2025). BC is a potent, broad-spectrum absorber, while BrC
30 exhibits strongly wavelength-dependent absorption, primarily in the near-ultraviolet to
31 visible range (Bond et al., 2013; Laskin et al., 2015). Accurately quantifying their
32 respective contributions to total light absorption is fundamental for assessing aerosol
33 radiative forcing, understanding atmospheric heating rates, and constraining climate
34 models (Li et al., 2023a; Yang et al., 2025; Zhu et al., 2021). A key complexity, however,
35 arises from the atmospheric ageing of BC. This process frequently results in the internal
36 mixing of BC with non-absorbing or weakly absorbing coatings and enhances BC's
37 absorption because of the lensing effect (Cappa et al., 2012; Jin et al., 2025; Yus-Díez
38 et al., 2022). Consequently, the total measured absorption coefficient of ambient
39 aerosols ($B_{\text{abs_coated}}$) is an aggregate signal from three distinct physical processes:
40 absorption by bare BC cores, absorption by BrC, and the lensing-driven enhancement
41 of BC absorption due to coatings. Thus, disentangling these three contributors—
42 referred to as apportionment of total aerosol light absorption—is essential for advancing
43 our understanding of aerosol mixing state, ageing processes, and ultimately, climate
44 impacts (Liu et al., 2015; Pokhrel et al., 2017).

45 However, most methodological frameworks attempting to decompose aerosol total
46 absorption could only resolve one or two of these contributors, but not all three. For
47 example, a common way to obtain the information of one contributor is by accounting
48 for the contributions of the other species based on their own known physicochemical
49 properties. These properties are usually solubility in water or organic reagents or
50 thermal stability at a certain temperature (Cappa et al., 2019; Liu et al., 2015; Xie et al.,
51 2019). For the former, BC light absorption can be obtained as organic species are
52 vaporized (Cappa et al., 2019; Liu et al., 2015; Xie et al., 2019) and for the latter, the
53 optical properties of solutions can be measured to estimate the light absorption of BrC



54 (Choudhary et al., 2017; Wu et al., 2019; Yue et al., 2019). Being inherently designed
55 to isolate a single component, these approaches typically focus on either BC or BrC
56 alone. Another approach for separating the contributions of BC and BrC from the total
57 measured aerosol light absorption is the absorption Ångström exponent (AAE)
58 attribution method (Lack and Langridge, 2013; Wang et al., 2019a, b). This approach
59 assumes that only BC absorbs solar radiation at near-infrared wavelengths (e.g., 880
60 nm) and the BC's AAE (AAE_{BC}) is 1.0 or other preset values. The light absorptions of
61 BC at other wavelengths ($B_{abs,BC}(\lambda)$) are extrapolated with the help of AAE_{BC} , enabling
62 the light absorption of BrC ($B_{abs,BrC}(\lambda)$) to be calculated by subtracting the $B_{abs,BC}(\lambda)$
63 from the measured total absorption ($B_{abs_coated}(\lambda)$). Considering that the AAE_{BC} value is
64 actually variable (Liu et al., 2018b; Wang et al., 2021b), this approach is not perfect yet.

65 Thus far, methodological frameworks capable of resolving all three contributors
66 include the applications of pure numerical calculation or the combination of a thermal
67 denuder with a photoacoustic soot spectrometer (PASS-3) in field measurements. The
68 former category is usually embedded with too many assumptions (Luo et al., 2018,
69 2021; Moschos et al., 2021; Zhang et al., 2021) and needs further improvement based
70 on field verifications. The latter includes the combined use of photoacoustic
71 spectroscopy (PAX) and thermal denuding (TD), which allows for the calculation of an
72 absorption enhancement factor (E_{abs}) and, with additional spectral constraints, the
73 separation of BrC and lensing contributions from BC (Cappa et al., 2012; Liu et al.,
74 2015; Pokhrel et al., 2017). Even if the TD process may be subject to an incomplete
75 separation of BrC from BC (Liu et al., 2015) and is therefore not conducive to an
76 accurate apportionment, it is still appreciable in distinguishing the absorption
77 contributors and calculating absorption enhancement factors.

78 In this study, we introduce and demonstrate an integrated methodological
79 framework designed to apportion total carbonaceous aerosol light absorption into its
80 three constituent parts. Two established but typically separate techniques: PAX and
81 integrating sphere with solvent extraction (ISS) are synergistically coupled to provide

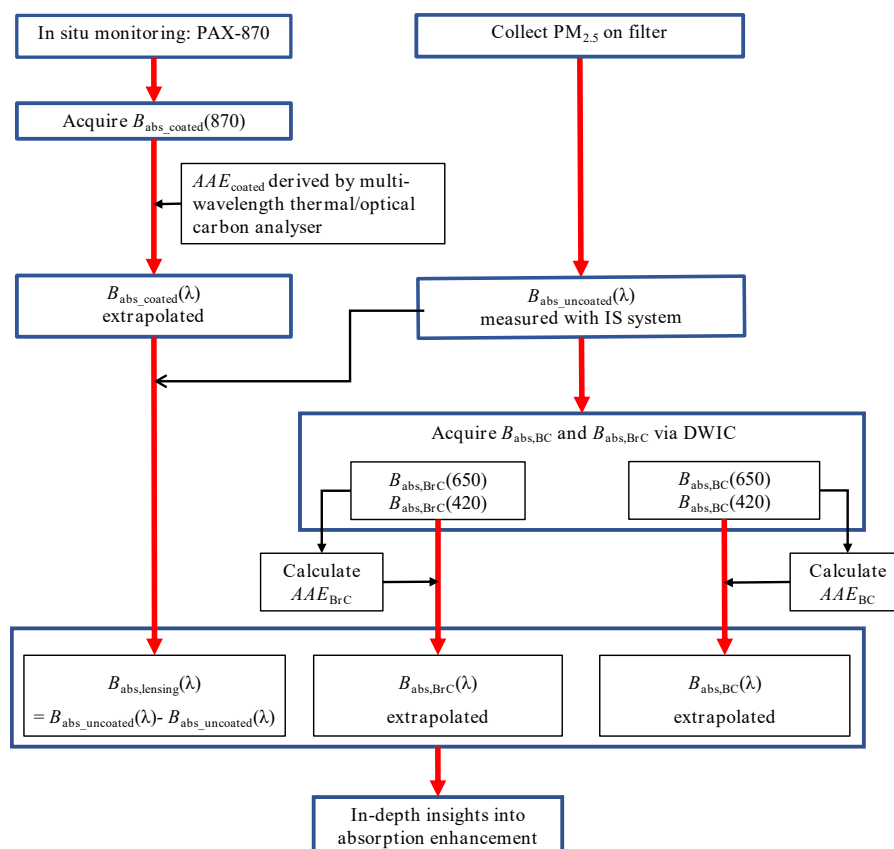


82 a self-consistent framework to apportion absorption to BC, BrC, and the lensing effect.
83 We present this methodology, detail its implementation, and demonstrate its
84 applications such as in the understanding of absorption enhancement due to absorptive
85 or non-absorptive coatings. We anticipate that this methodology will provide robust
86 constraints for aerosol optical properties and climate modelling.

87 2 Methodology

88 2.1 Methodological architecture

89 As mentioned in the Introduction, the methodology adopted here is based on coupling
90 two mature techniques: PAX and ISS. The PAX provides an accurate, in situ
91 measurement of the total ambient absorption coefficient at 870 nm ($B_{\text{abs_coated}}(870)$)
92 (Lack et al., 2012; Selimovic et al., 2019). This value is subsequently extrapolated to
93 derive absorption coefficients across wavelengths from 380 nm to 880 nm ($B_{\text{abs_coated}}(\lambda)$).
94 Concurrently, the ISS system measures the absorption of the same aerosol population
95 after the lensing effect has been eliminated by solvent-mediated coating removal and
96 refractive index matching, yielding $B_{\text{abs_uncoated}}(\lambda)$. The reason why the mixed solvent
97 eliminate lensing has been detailed in a few publications (Li et al., 2023b; Sun et al.,
98 2021; Wonaschütz et al., 2009). The difference [$B_{\text{abs_coated}}(\lambda) - B_{\text{abs_uncoated}}(\lambda)$] directly
99 quantifies the absorption enhancement due solely to the lensing effect ($B_{\text{abs,lensing}}(\lambda)$).
100 Furthermore, the ISS system, employing a Double-Wavelength Iterative Calculation
101 (DWIC) algorithm with carbon black and humic acid as reference materials, spectrally
102 decomposes $B_{\text{abs_uncoated}}(\lambda)$ into the contributions of bare BC ($B_{\text{abs,BC}}$) and BrC ($B_{\text{abs,BrC}}$)
103 (Sun et al., 2021; Wonaschütz et al., 2009). A schematic of the methodological
104 architecture is shown in Figure 1.



105

106

Figure 1. Methodological architecture. Note: The λ ranges from 370 nm to 880 nm

107

2.2 Measurement of lensing-free absorption using ISS system

108

2.2.1 Sample collection

109

Ambient $PM_{2.5}$ (particulate matter with an aerodynamic diameter $\leq 2.5 \mu m$) was

110

sampled at the Chinese Research Academy of Environmental Sciences (CRAES),

111

Beijing (40.04°N, 116.42°E). A high-volume air sampler (Tisch Environmental Inc.,

112

OH, USA) was used at an air flow rate of 1.13 m^3/min . The sampling site was situated

113

atop a smog chamber facility (~ 10 m above ground), with an 80-meter radius free of

114

anthropogenic emission sources nearby (Li et al., 2023b; Wang et al., 2021a; Zhang et

115

al., 2020). Quartz fibre filters (Pallflex™ Tissuquartz 2500QAT-UP, 8" \times 10", Pall

116

Corporation) were deployed for 23.5-hour repeated sampling cycles, commencing at

117

09:00 Beijing Time (UTC+8) every day and concluding at 08:30 the following morning.



118 Seasonal campaigns in 2023 spanned the winter period of 9–24 February, the spring
119 period of 7 April–9 May, the summer period of 7 July–6 August, and the autumn period
120 of 12 October–5 November. The selected four time periods are representative of the
121 meteorological conditions and emission regimes of four quarters of the year (Li et al.,
122 2023b; Wang et al., 2021a; Zhang et al., 2020). The quality assurance measures for
123 sampling filters and eligible days (Table S1) are detailed in Supporting Information
124 (Sect. S1).

125 2.2.2 Measurement of absorption for uncoated aerosol

126 As previously described, the ISS system eliminates lensing-induced absorption
127 ($B_{\text{abs,lensing}}(\lambda)$) while preserving bare BC and BrC absorption components (i.e.,
128 $B_{\text{abs,uncoated}}(\lambda) = B_{\text{abs,BC}}(\lambda) + B_{\text{abs,BrC}}(\lambda)$) (Sun et al., 2017; Wonaschütz et al.,
129 2009; Li et al., 2023). The system comprises a light source, a custom-made 150 mm IS,
130 and a UV–Vis–NIR spectrometer (Li et al., 2023b; Sun et al., 2017, 2021; Wang et al.,
131 2021a). For each measurement, a transparent quartz cuvette (1 cm × 1 cm × 4 cm),
132 holding 3 mL of a solvent mixture (acetone, water, and 2-propanol in a ratio of 5:4:1)
133 was fixed in the center of the integrating sphere chamber. A filter punch (30×8 mm)
134 was immersed in the solvent mixture within the cuvette for optical detection. The
135 wavelength-resolved absorbance ($ABS_{\text{ISS}}(\lambda)$) was acquired from 370 nm to 880 nm,
136 defined as:

$$137 \quad ABS_{\text{ISS}}(\lambda) = -\ln \frac{I(\lambda)}{I_0(\lambda)}, \quad (1)$$

138 where $I(\lambda)$ and $I_0(\lambda)$ denote the transmitted light intensities through the loaded and blank
139 filters, respectively. The absorption coefficient of uncoated aerosols ($B_{\text{abs,uncoated}}(\lambda)$) is
140 then converted as:

$$141 \quad B_{\text{abs,uncoated}}(\lambda) = \frac{100 \times ABS_{\text{ISS}} \times A}{CF \times F \times T}, \quad (2)$$

142 where A is the total deposited area on the filter used by the high-volume sampler
143 described in Sect. 2.2.1 (cm^2); F is the flow rate of filter sampling (m^3/min); T is the
144 duration of each filter sampling (min); and CF is the correction factor converting the
145 ISS-measured absorption (multiple-angle absorption within the integrating sphere



146 chamber) to the conventional one-way absorption (as measured by PAX). The method
147 for determining the CF value has been described in our previous publication (Li et al.,
148 2023b) and is represented in Supporting Information (Sect. S2).

149 2.3 Measurement of total absorption via PAX

150 2.3.1 Thermal/optical analysis

151 A DRI Model 2015 Multi-Wavelength Thermal-Optical Carbon Analyser was used to
152 split aerosol total carbon (TC) into organic carbon (OC) and elemental carbon (EC)
153 employing temperature-regulated pyrolysis under controlled atmospheres. A 0.5024
154 cm² punch from a quartz filter was heated stepwise to 140 °C (OC1), 280 °C (OC2),
155 480 °C (OC3), and 580 °C (OC4) in a pure helium atmosphere and then combusted
156 stepwise at 580 °C (EC1), 740 °C (EC2), and 840 °C (EC3) in a 2% oxygen + 98%
157 helium atmosphere following the IMPROVE_A temperature protocol. The mass values
158 of OC and EC were calculated as $OC = OC1 + OC2 + OC3 + OC4 + OPC$ and $EC =$
159 $EC1 + EC2 + EC3 - OPC$, where OPC represents pyrolyzed OC (Chow et al., 2007).

160 To acquire $AAEs$, filter transmittance and reflectance were continuously monitored
161 using 7-wavelength diode lasers (405, 445, 532, 635, 780, 808, 980 nm), and the
162 wavelength-specific light attenuation (ATN) was calculated accordingly. To mitigate
163 filter matrix artefacts, including loading effects and multiple scattering (Chen et al.,
164 2015; Chow et al., 2018; Peng et al., 2020), wavelength- and EC loading-dependent
165 adjustment factors were applied to the raw ATN to obtain corrected $ATNs$ (see
166 Supporting Information Sect. S3, Table S2). Based on these, the $AAEs$ for coated
167 aerosols (AAE_{coated}) were calculated. The AAE_{coated} was then used to extrapolate
168 $B_{\text{abs_coated}}(\lambda)$ from $B_{\text{abs_coated}}(870)$ in the following section.

169 2.3.2 Acquisition of total absorption at broad wavelength range

170 A photoacoustic extinction spectrometer (PAX-870, Droplet Measurement
171 Technologies) was deployed to monitor the in situ atmospheric absorption coefficient
172 at 870 nm ($B_{\text{abs_coated}}(870)$) in real-time. Considering that we have only a PAX set with
173 a single wavelength (870 nm), the absorption coefficients at other wavelengths



174 ($B_{\text{abs_coated}}(\lambda)$) had to be extrapolated using the AAE_{coated} obtained in Sect. 2.3.1:

$$175 \quad B_{\text{abs_coated}}(\lambda) = B_{\text{abs_coated}}(870) \times \left(\frac{\lambda}{870}\right)^{-AAE_{\text{coated}}} \quad (3)$$

176 2.4 Decomposition of coated aerosol absorption by coupling ISS-PAX

177 2.4.1 Lensing-equivalent absorption

178 The availability of $B_{\text{abs_coated}}(\lambda)$ from PAX and $B_{\text{abs_uncoated}}(\lambda)$ from ISS allows the
 179 acquisition of $B_{\text{abs,lensing}}(\lambda)$. As shown in Figure 1, $B_{\text{abs,lensing}}(\lambda)$ is obtained by calculating
 180 the difference between $B_{\text{abs_coated}}(\lambda)$ and $B_{\text{abs_uncoated}}(\lambda)$, as:

$$181 \quad B_{\text{abs,lensing}}(\lambda) = B_{\text{abs_coated}}(\lambda) - B_{\text{abs_uncoated}}(\lambda) \quad (4)$$

182 2.4.2 BC and BrC absorptions

183 To decompose $B_{\text{abs_uncoated}}(\lambda)$, which is lensing free, into the individual contributions of
 184 BC and BrC, the DWIC algorithm was employed. Details of the DWIC algorithm have
 185 been described in our previous publications (Sun et al., 2017, 2021; Wang et al., 2021a)
 186 and in the Supporting Information (Sect. S4 and Figure S1). Briefly, the iterative
 187 calculation uses two wavelengths (650 and 420 nm) and two reference materials:
 188 Carbon Black (CarB) as the proxy for BC, and Humic Acid Sodium Salt (HASS) as the
 189 proxy for BrC (Reisinger et al., 2008; Sun et al., 2017; Wang et al., 2021a, a;
 190 Wonaschütz et al., 2009). Calibration curves for CarB and HASS masses were
 191 established based on their respective absorption signals measured by the ISS at 650
 192 (BC-dominated) and 420 nm (BrC-sensitive). Iterative optimization yielded the
 193 absorption coefficients of BC and BrC at these two wavelengths, i.e., $B_{\text{abs,BC}}(650)$,
 194 $B_{\text{abs,BC}}(420)$, $B_{\text{abs,BrC}}(650)$, and $B_{\text{abs,BrC}}(420)$.

195 The absorption coefficients of BC and BrC at wavelengths other than 420 nm and
 196 650 nm (i.e., $B_{\text{abs,BC}}(\lambda)$, $B_{\text{abs,BrC}}(\lambda)$) can be extrapolated from the values at these two
 197 wavelengths, constrained by their respective $AAEs$ (AAE_{BC} and AAE_{BrC}). The AAE for
 198 BC or BrC is calculated as:

$$199 \quad AAE_X = -\frac{\ln\left(\frac{B_{\text{abs},x}(650)}{B_{\text{abs},x}(420)}\right)}{\ln\frac{650}{420}} \quad (5)$$



200 The absorption coefficient at any wavelength is then given by:

$$201 \quad B_{\text{abs},x}(\lambda) = B_{\text{abs,uncoated}}(420) \times \left(\frac{\lambda}{420}\right)^{-AAE_x} \quad (6)$$

202 where X refers to BC or BrC. The wavelength 420 nm in Eq. (6) can be replaced by

203 650 nm.

204 2.5 Calculation of absorption enhancement factors

205 With the total aerosol absorption apportioned to BC, BrC, and lensing effect, the

206 absorption enhancement factor of BC ($E_{\text{abs}}(\lambda)$) is available via:

$$207 \quad E_{\text{abs}}(\lambda) = \frac{B_{\text{abs,BC}}(\lambda) + B_{\text{abs,lensing}}(\lambda)}{B_{\text{abs,BC}}(\lambda)} \quad (7)$$

208 3 Results and discussion

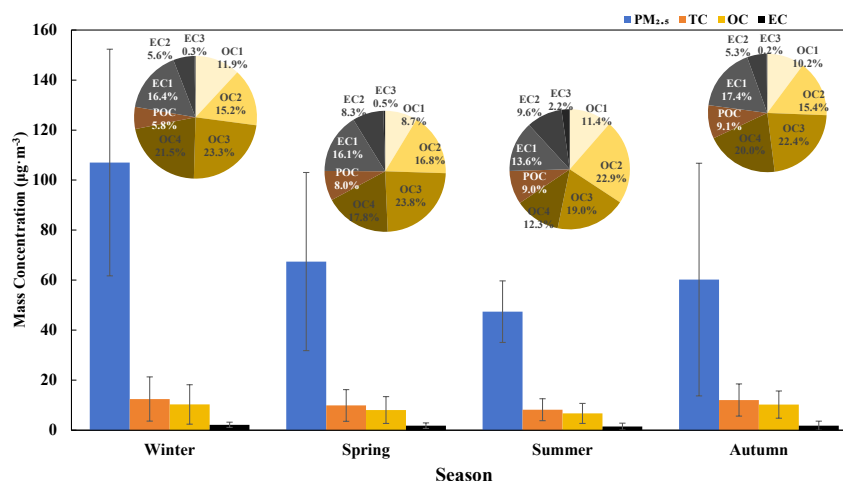
209 3.1 Concentrations and total absorptions of ambient aerosol

210 3.1.1 Concentrations

211 Every filter-collected sample was weighed to determine $\text{PM}_{2.5}$ concentration and

212 analysed for aerosol carbon speciation (Figure 2). Representative seasonal

213 heterogeneity was observed in aerosol loadings and compositions.



214

215

Figure 2. Aerosol loadings and compositions in 2023.

216

As shown in Figure 2, $\text{PM}_{2.5}$ mass concentrations demonstrate pronounced

217 seasonal variations, peaking in winter ($107.03 \pm 45.31 \mu\text{g}\cdot\text{m}^{-3}$) and reaching a minimum

218 in summer ($47.40 \pm 12.30 \mu\text{g}\cdot\text{m}^{-3}$), consistent with regional emission patterns and

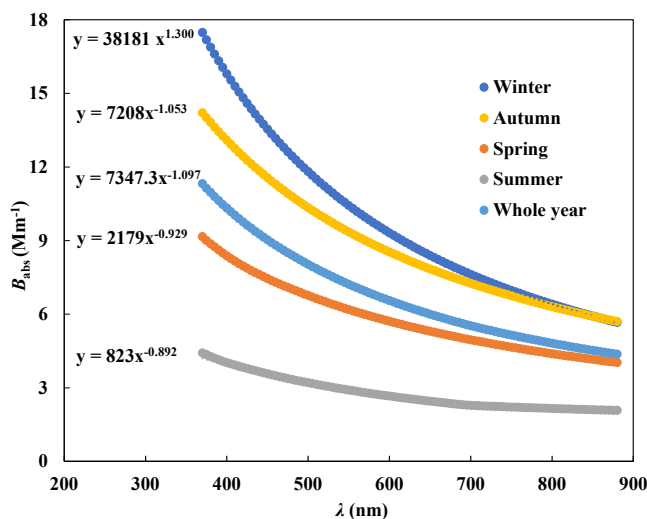


219 meteorological conditions (Chen et al., 2017; Wu et al., 2016b). The seasonal trends in
220 TC, OC, and EC concentrations generally mirrored those of $PM_{2.5}$, although the relative
221 order of spring and autumn was occasionally reversed. For example, unlike $PM_{2.5}$
222 concentrations of spring > autumn, EC concentrations are of autumn > spring, implying
223 differences in $PM_{2.5}$ composition arising from varied sources, transport, and ageing
224 processes (Arhami et al., 2018; Ravindra et al., 2022; Song et al., 2022).

225 Thermal-optical carbon analysis provided distinct source signatures, as indicated
226 by the char-EC/soot-EC ratios. Elevated ratios during high-combustion seasons like
227 winter (1.81 ± 1.61) and autumn (1.50 ± 2.67) reflect predominant contributions from
228 coal and biomass burning, as established by source apportionment studies (e.g., Han et
229 al., 2010). In contrast, reduced ratios during spring (0.93 ± 0.77) and summer ($0.39 \pm$
230 0.58) accord with vehicular-dominated emissions (Han et al., 2008; Liu et al., 2018a).
231 Further speciation of OC to OC1, OC2, OC3, and OC4 suggests the influence of
232 atmospheric processing. Low-volatility OC3–OC4 fractions constitute 40–54% of total
233 OC across all seasons, indicating the pathways of photochemical ageing and aqueous-
234 phase processing that generate oxygenated semi-volatile compounds (Aswini et al.,
235 2019; Li et al., 2018).

236 3.1.2 Total absorption

237 Having established the mass concentration and compositional context, we now examine
238 the optical absorption properties of the coated aerosols. The daily light absorption of
239 coated aerosol calculated in Sect. 2.3.2 was averaged seasonally and annually. Figure 3
240 shows the spectral dependence of total light absorption ($B_{\text{abs_coated}}(\lambda)$) across seasons
241 and the annual average. Both the absorption intensity and the absorption Ångström
242 exponent (AAE_{coated}) exhibit a consistent seasonal order: winter > autumn > spring >
243 summer. This order aligns with the seasonal trend in TC concentrations shown in Figure
244 2. Since both BC and BrC are spectrally dependent components of TC, it is consistent
245 that the AAE_{coated} values follow the same order as TC concentrations.



246

247

Figure 3. Total absorption of coated aerosol.

248 The AAE_{coated} values were highest in winter (1.300) and lowest in summer (0.892),
 249 with an annual mean of 1.053. $AAEs$ lower than 1.0 are observed in spring and summer,
 250 seemingly challenging the traditional view that the AAE of carbonaceous aerosol should
 251 exceed 1.0, given that BC 's AAE is typically 1.0 and BrC 's $AAE > 1.0$ (Lack and
 252 Langridge, 2013). However, previous source-related experiments and Mie model
 253 calculations (Li et al., 2016; Liu et al., 2018b; Wang et al., 2021b) have reported a wide
 254 range of values for AAE_{BC} (e.g., 0.6–1.6) due to various confounding factors, implying
 255 the possibility of AAE values below 1.0 for coated aerosol. While referencing this broad
 256 range is instructive, the consistently low AAE_{coated} values in our spring and summer data
 257 may also be partially influenced by the net spectral effect of lensing enhancement and
 258 BrC blocking, which our subsequent deconvolution analyses aim to clarify.

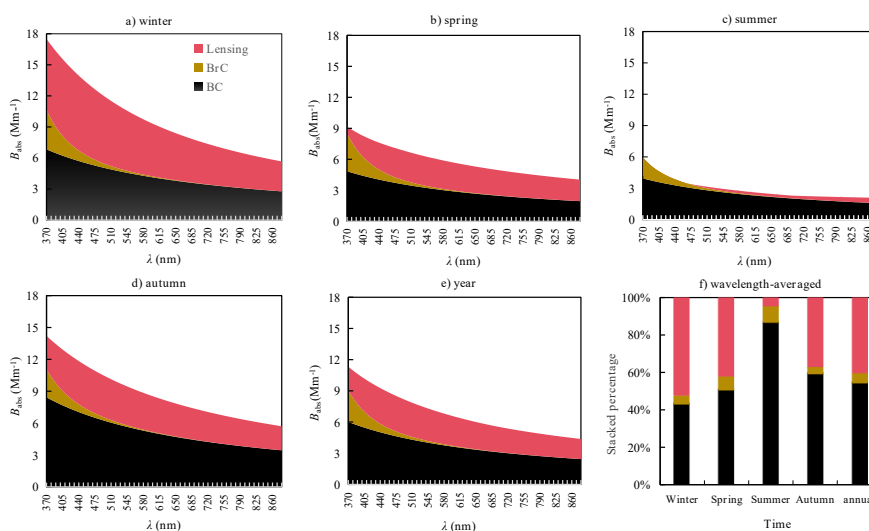
259 To sum up this section (Sect. 3.1), the distinct seasonal characteristics of aerosol
 260 concentrations, carbon ratios, and $AAEs$ reflect the diversity of the local ambient aerosol
 261 population, providing a suitable context for a comprehensive study of overall and
 262 decomposed light absorptions using the PAX-ISS hybrid method.

263 3.2 Deconvolved light absorption

264 Total absorption ($B_{\text{abs_coated}}(\lambda)$) was deconvolved into $B_{\text{abs},BC}(\lambda)$, $B_{\text{abs},BrC}(\lambda)$, and



265 $B_{\text{abs,lensing}}(\lambda)$ on daily, seasonal, and annual bases. Figure 4 shows the seasonal and
 266 annual decomposed absorption, where panels a–d display the wavelength-resolved
 267 contributions for winter, spring, summer, and autumn, respectively; panel e shows the
 268 annual wavelength-resolved contribution; and panel f shows the wavelength-averaged
 269 contributions for each season and the whole year. As noted, the wavelength range
 270 considered spans 370–880 nm, representing a most energetic part of solar radiation
 271 (Thuillier et al., 2003). To enable direct comparison across time periods, all panels
 272 showing wavelength-resolved absorptions (a–e) share a common y-axis upper limit of
 273 18 Mm^{-1} .



274

275 **Figure 4.** Deconvolved aerosol light absorption in wavelength-resolved (a–e) and wavelength-averaged (f) forms.

276 Both BC and BrC exhibited clear spectral dependence seasonally and annually
 277 (panels a–e), with BrC’s dependence being more pronounced than BC’s, consistent
 278 with the established knowledge that $AAE_{\text{BrC}} > AAE_{\text{BC}}$ (Kaskaoutis et al., 2021; Lack and
 279 Langridge, 2013; Wu et al., 2016a). In all seasons, BC absorption exceeded BrC
 280 absorption even at ultraviolet wavelengths, indicating BC’s dominant role in light
 281 absorption for the urban aerosol studied. This is further corroborated by Figure 4f,
 282 where the wavelength-averaged BrC absorption value was approximately 10% of BC
 283 absorption value for both individual seasons and the annual average. Regarding the



284 apparent lensing-equivalent absorption ($B_{\text{abs,lensing}}$), Figure 4f shows an annual mean
285 contribution of 40.0% to the total light absorption ($B_{\text{abs_coated}}$), with seasonal means of
286 52.0% in winter, 41.8% in spring, 4.6% in summer, and 36.7% in autumn. These
287 differing seasonal contributions of $B_{\text{abs,lensing}}$ suggest varying degrees of BC absorption
288 enhancement, discussed in Sect. 3.3.

289 More significantly, and central to one of our key findings, Figure 4a–e reveals a
290 pronounced contraction of the apparent lensing effect toward shorter wavelengths. For
291 example, at the annual level (Figure 4e), the lensing-equivalent absorption at 370 nm
292 was only 66.3% of its maximum value at 455 nm. In spring (Figure 4b), lensing-
293 equivalent absorption at 370 nm shrank to 22.9% of the maximum at 505 nm. The most
294 extreme case was observed in summer (Figure 4c), where the lensing-equivalent
295 absorption disappears at wavelengths below 465 nm. In this scenario, the summed
296 absorption of BC and BrC at specific wavelengths (e.g., below 465 nm) exceeded the
297 total measured absorption (summed absorption of BC, BrC, and lensing), suggesting
298 that the intrinsic total lensing effect ($B_{\text{abs,Tlensing}}$) was overbalanced by other factors to
299 the extent that the apparent lensing effect ($B_{\text{abs,lensing}}$) became negligible or negative.
300 Although an accurate and reliable explanation for this spectral contraction phenomenon
301 remains unavailable, the multiple effects of BrC internally mixed with BC cores are
302 attracting increasing attention. Generally, coatings on BC can enhance its absorption
303 via the lensing effect. When coatings are themselves absorptive (e.g., BrC), this
304 enhancement constitutes one of the largest uncertainties in estimating aerosol radiative
305 forcing (e.g., Curci et al., 2019; Wang et al., 2018). It has been established that the
306 absorption enhancement of BC due to absorptive coatings (BrC) is lower than that
307 induced by non-absorbing coatings (Lack and Cappa, 2010).

308 Further studies propose classifying BrC's impacts on BC absorption into a BrC-
309 induced lensing effect and a BrC blocking effect (Luo et al., 2018; Zhang et al., 2021).
310 In our framework, the lensing effect caused by BrC combines with that from non-
311 absorbing coatings to constitute the intrinsic total lensing-equivalent absorption



312 ($B_{\text{abs,Tlensing}}$). The blocking effect ($B_{\text{abs,blocking}}$) occurs when BrC coatings block some
313 photons that would otherwise be focused onto the BC core by the lensing effect, akin
314 to a shadow. Therefore, total aerosol absorption should be defined as:

$$315 \quad B_{\text{abs_coated}} = B_{\text{abs,BC}}(\lambda) + B_{\text{abs,BrC}}(\lambda) + \left(B_{\text{abs,Tlensing}}(\lambda) - B_{\text{abs,blocking}}(\lambda) \right) \quad (8)$$

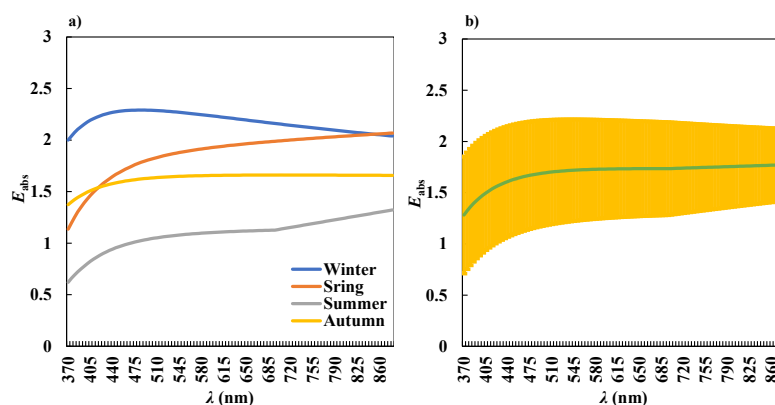
316 Consequently, the apparent lensing effect ($B_{\text{abs,lensing}}$) we measure represents the net
317 balance between total lensing enhancement ($B_{\text{abs,Tlensing}}(\lambda)$) and BrC blocking
318 ($B_{\text{abs,blocking}}$). Accordingly, $B_{\text{abs,lensing}}(\lambda)$ becomes negative whenever $B_{\text{abs,blocking}}(\lambda)$
319 exceeds $B_{\text{abs,Tlensing}}(\lambda)$. Thus, the observed contraction of $B_{\text{abs,lensing}}$ in Figure 4, which is
320 precisely ($B_{\text{abs,Tlensing}} - B_{\text{abs,blocking}}$), is not surprising. The disappearance of $B_{\text{abs,lensing}}(\lambda)$
321 in summer below 465 nm (Figure 4c) likely does not indicate the absence of intrinsic
322 total lensing but rather suggests that $B_{\text{abs,Tlensing}}(\lambda) - B_{\text{abs,blocking}}(\lambda) \leq 0$. The plausibility
323 of such a BrC-induced blocking effect is supported by prior numerical investigations.
324 For instance, Luo et al. (2018), employing the multiple-sphere T-matrix (MSTM)
325 method, demonstrated that the total absorption of a BC core with brown coatings can
326 be less than the sum of separately calculated absorptions ($B_{\text{abs,BC}} + B_{\text{abs,BrC}}$), attributable
327 to blocking. Similarly, Zhang et al. (2021) numerically found that the lensing effect may
328 not increase further with shell/core ratio beyond a threshold due to blocking.
329 Furthermore, the wavelength dependence of the apparent lensing in Figure 4 (apparent
330 lensing decreases toward shorter wavelengths) is largely complementary to that of BrC
331 absorption (BrC absorption increases toward shorter wavelengths), implying an
332 interplay with BrC blocking effects. Further investigations are needed to clarify the
333 conditions for blocking effects, their interaction with the lensing from non-absorptive
334 coatings, and their relationship with the direct light absorption from BrC.

335 3.3 Insight into absorption enhancement

336 The absorption enhancement of BC due to lensing is considered one of the largest
337 uncertainties in assessing the climate impact of aerosol light absorption (Fan et al., 2024;
338 Kong et al., 2024; Zhao et al., 2021). Here, we examine absorption enhancement from
339 both wavelength-resolved and wavelength-averaged perspectives, followed by a



340 discussion of why some enhancement quantification methods require correction.
 341 3.3.1 Wavelength-resolved enhancement: insight into blocking effects
 342 Using the daily wavelength-resolved absorption coefficients of BC, BrC, and apparent
 343 lensing effect (i.e., $B_{\text{abs,BC}}(\lambda)$, $B_{\text{abs,BrC}}(\lambda)$, and $B_{\text{abs,lensing}}(\lambda)$) obtained via Eqs. (4) and (6),
 344 the daily, seasonal, and annual wavelength-resolved enhancement factors ($E_{\text{abs}}(\lambda)$) were
 345 calculated using Eq. (7).



346

347

Figure 5. for seasonal (a) and yearly (b) terms.

348 Figure 5 shows the wavelength-resolved enhancement factors for the seasons and
 349 the year. A clear wavelength dependence is evident. Specifically, $E_{\text{abs}}(\lambda)$ decreased
 350 monotonically toward shorter wavelengths in spring, summer, and autumn, while in
 351 winter it increased initially before declining in the short-wavelength range. That is, all
 352 seasonal and annual $E_{\text{abs}}(\lambda)$ values turned downward as wavelengths approached the
 353 violet range. The observed decline in $E_{\text{abs}}(\lambda)$ is mechanistically explained by the
 354 definition of E_{abs} ($E_{\text{abs}} = 1 + B_{\text{abs,lensing}}/B_{\text{abs,BC}}$) given the concurrent decrease in $B_{\text{abs,lensing}}$
 355 (Figure 5) and the increase in $B_{\text{abs,BC}}$ at shorter wavelengths (Figure 4). This decline in
 356 E_{abs} at short wavelengths is thus fundamentally driven by the strengthened blocking
 357 effect of BrC coatings, which reduces the net apparent lensing ($B_{\text{abs,lensing}} = B_{\text{abs,Tlensing}} -$
 358 $B_{\text{abs,blocking}}$). The most extreme case occurred in summer at wavelengths below 465 nm,
 359 where observed $E_{\text{abs}}(\lambda)$ values fell below 1.0, indicating that the net apparent lensing
 360 contributed negatively to BC light absorption. This echoes the finding of Luo et al.



361 (2018) that $E_{\text{abs}}(\lambda)$ can be below 1 in the ultraviolet region for BC with brown coatings
362 due to blocking, which they termed the “sunglasses effect”. While the blocking effect
363 of BrC has previously been examined only through numerical simulations (e.g., Luo et
364 al., 2018; Zhang et al., 2021), our study provides the first field-based evidence to
365 demonstrate this phenomenon.

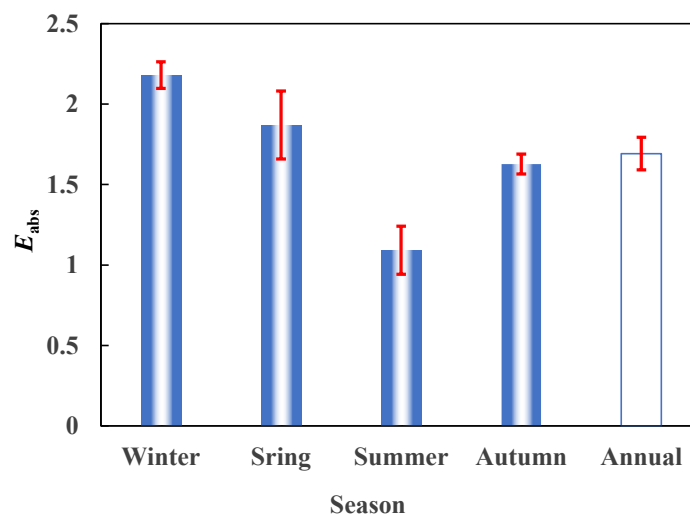
366 3.3.2 Wavelength-averaged enhancement: insight into pollution- 367 enhancement linkage

368 Theoretical and experimental studies of lensing-induced absorption enhancement have
369 yielded diverse results. Mie theory for spherical core-shell particles yields enhancement
370 factors up to 3 (Bond et al., 2006; Jacobson, 2001; Schwarz et al., 2008). Such
371 enhancement is supported by laboratory studies (Cappa et al., 2012; Schnaiter, 2005;
372 Shiraiwa et al., 2010; Zhang et al., 2008) and is incorporated into climate models that
373 work out total BC absorption (lensing included) either through simplified mixing-state
374 assumptions (Chung, 2005; Penner et al., 1998) or by fixing the enhancement value at
375 ~ 1.5 (Flanner et al., 2007; Wang et al., 2014). In contrast, some field measurements
376 have reported negligible absorption enhancement for ambient BC particles (Cappa et
377 al., 2012, 2019; Fierce et al., 2016; Mbengue et al., 2021).

378 Complementing the wavelength-resolved results, we present the wavelength-
379 averaged enhancement factor (E_{abs} , averaged over 370-880 nm) to assess the overall
380 status of lensing. As shown in Figure 6, the annual average E_{abs} was 1.69 ± 0.10 .
381 Seasonal averages varied from 1.09 ± 0.15 (summer) to 2.18 ± 0.08 (winter), with spring
382 and autumn values of 1.81 ± 0.21 and 1.63 ± 0.06 , respectively. Given the decisive role
383 of lensing, the considerable seasonal divergence in E_{abs} is attributable to the varying
384 contributions of apparent lensing ($B_{\text{abs,lensing}}$) to total absorption ($B_{\text{abs,coated}}$) (e.g., 4.6%
385 in summer versus 52.0% in winter; see Figure 4f). Other researchers have also reported
386 diverse absorption enhancement factors in China, depending on specific conditions
387 influencing lensing, particularly aerosol ageing statuses (Luo et al., 2018). For example,
388 Cui et al. (2016) reported factors of 1.4 ± 0.3 for fresh combustion and ~ 3 for aged BC



389 at a rural North China Plain site. Chen et al. (2017) reported an average of 2.07 ± 0.72
390 for winter haze in northern China, with diurnal variation from 1.31 ± 0.29 (morning) to
391 2.23 ± 1.05 (afternoon) and 1.52 ± 0.75 (evening). Xu et al. (2016) even reported E_{abs}
392 values of 2.6–4.0 for Beijing.



393

394

Figure 6. Wavelength-averaged absorption enhancement factors for seasons and the year.

395 Beyond the comparison with literature values, a notable pattern emerges within
396 our dataset: the seasonal E_{abs} values (Figure 6) vary synchronously with $\text{PM}_{2.5}$
397 concentrations (Figure 2); that is, higher $\text{PM}_{2.5}$ levels corresponded to higher absorption
398 enhancement factors. This aligns with our previous findings that increased air pollution
399 leads to greater absorption enhancement (Li et al., 2023b; Zhang et al., 2017, 2020; Zhi
400 et al., 2014). Increased air pollution in northern China usually results from stagnant
401 weather that favors aerosol ageing, leading to the accumulation of primary emissions
402 and the formation of secondary aerosols (Liu et al., 2024; Peng et al., 2021). The
403 increased load of inorganic and organic pollutants enhances the likelihood and thickness
404 of coatings on BC, thereby boosting the lensing effect (Li et al., 2023b).

405 This positive correlation is supported by the enhanced abundance of low-volatility,
406 oxidised organic components (OC3-OC4, see Figure 2) during the high- $\text{PM}_{2.5}$ seasons
407 (winter and autumn). These components are markers of atmospheric ageing and



408 secondary formation (Boonpeng et al., 2026; Chow et al., 2007; Tohidi et al., 2022),
409 processes conducive to the development of thicker coatings on BC, thereby promoting
410 a stronger lensing effect.

411 With sustained improvements in local air quality in China, conflicting climate
412 influences may emerge: the warming effect could weaken due to a continued decline of
413 E_{abs} , while the cooling effect from aerosol scattering could also weaken due to declining
414 $\text{PM}_{2.5}$ concentration (Kelesidis et al., 2022; Samset et al., 2025; Xie et al., 2025). Future
415 work should address this potential contradiction.

416 **4 Conclusions**

417 This study developed and applied a novel hybrid measurement method, coupling in situ
418 PAX with filter-based ISS, to quantitatively apportion ambient aerosol light absorption
419 into contributions from BC, BrC, and the lensing effect. The method successfully
420 provided a self-consistent, observationally constrained pathway to separate these three
421 components, addressing a persistent challenge in atmospheric aerosol science.

422 Key findings from the annual and seasonal analysis of Beijing aerosols in 2023
423 include:

424 **(1) Successful apportionment:** The PAX-ISS method successfully deconvolved
425 the total absorption, confirming BC as the dominant absorber. BrC contributed
426 approximately 10% to the annual wavelength-averaged absorption, highlighting its
427 non-negligible role even in an urban environment.

428 **(2) Spectral Nature and Seasonal Variability of Lensing:** The lensing-induced
429 enhancement accounted for an annual average of 40.0% of total absorption but showed
430 profound seasonal variability (winter: 52.0%; summer: 4.6%). Crucially, the apparent
431 lensing effect ($B_{\text{abs,lensing}}$) exhibited strong spectral dependence, contracting
432 significantly at shorter wavelengths (UV/blue). This contraction is inconsistent with a
433 purely additive lensing model.

434 **(3) Observational Evidence for the BrC Blocking Effect:** The observed spectral
435 contraction, particularly the near-zero or negative apparent lensing at short wavelengths



436 in summer, provides compelling field-based evidence for a “blocking effect” caused by
437 absorptive BrC coatings on BC cores. This effect partially offsets the traditional lensing
438 enhancement, leading to the net apparent lensing captured by our method ($B_{\text{abs,lensing}} =$
439 $B_{\text{abs,Tlensing}} - B_{\text{abs,blocking}}$). Our results align with and provide tangible support for
440 previous theoretical and numerical studies proposing this mechanism.

441 **(4) Absorption Enhancement Factors and Pollution Linkage:** The derived
442 wavelength-averaged BC absorption enhancement factor (E_{abs}) varied seasonally from
443 1.09 ± 0.15 (summer) to 2.18 ± 0.08 (winter), with an annual mean of 1.69 ± 0.10 . These
444 values correlated with seasonal $\text{PM}_{2.5}$ levels, linking stronger enhancement to more
445 polluted, aged aerosol conditions.

446 **(5) Caveats and limitations:** The PAX-ISS hybrid method offers a powerful tool
447 for deconvolving the complex sources of aerosol absorption without requiring detailed
448 assumptions or information about particle microphysical properties, such as size
449 distributions, morphology, mixing state, or core-shell structure. This characteristic is,
450 on one hand, an advantage over methods that rely on such parameters. On the other
451 hand, it constitutes a limitation, as our framework currently cannot directly link the
452 observed absorption enhancement to these fundamental particle properties. For instance,
453 while particle size critically influences the magnitude and spectral dependence of
454 absorption enhancement (e.g., Chen et al., 2025; Fu et al., 2024), our approach does not
455 provide size-resolved insights. To address this, we have included the aerosol size
456 distribution data, simultaneously measured with a Scanning Mobility Particle Sizer
457 (SMPS), in our accompanying data set (see <https://doi.org/10.5281/zenodo.18552344>,
458 Shen et al., 2026) for reference by the community. Future research should aim to
459 integrate such size-resolved measurements and multi-component characterizations (e.g.,
460 PAX coupled with a thermal denuder (Cappa et al., 2012; Liu et al., 2015; Pokhrel et
461 al., 2017), SP2 (Dahlkötter et al., 2014), or VTDMA (Zhang et al., 2016)) to better
462 constrain the dependence of absorption enhancement on microphysical and
463 compositional variables.



464

465 **Data availability.** The primary data used in this study can be obtained from
466 <https://doi.org/10.5281/zenodo.18552344> (Shen et al., 2026). In addition, we include
467 the aerosol size data we simultaneously observed using an SMPS into above data set
468 for reference. Other data utilized in the present study are available from the
469 corresponding author on request.

470

471 **Author contributions.** Guorui Zhi and Yuzhe Zhang designed the research. Yi Shen
472 and Guorui Zhi wrote the paper. Yi Shen, Wenjing Jin, Yao Kong, and Yuzhe Zhang
473 carried out the field measurements. Yi Shen, Wenjing Jin, Yao Kong, Yuzhe Zhang,
474 Zhengying Li, and Jianzhong Sun analyzed the data. Yuankai Wang and Zhijian Liang
475 helped with the interpretation of the results.

476

477 **Competing interests.** The authors declare that they have no conflict of interest.

478

479 **Financial support.** This study was supported by the National Natural Science
480 Foundation of China (grant nos. 42477275, 41977309).

481



482 **References**

- 483 Arhami, M., Shahne, M. Z., Hosseini, V., Roufigar Haghighat, N., Lai, A. M., and
484 Schauer, J. J.: Seasonal trends in the composition and sources of PM_{2.5} and
485 carbonaceous aerosol in Tehran, Iran, *Environ. Pollut.*, 239, 69–81,
486 <https://doi.org/10.1016/j.envpol.2018.03.111>, 2018.
- 487 Aswini, A. R., Hegde, P., Nair, P. R., and Aryasree, S.: Seasonal changes in
488 carbonaceous aerosols over a tropical coastal location in response to
489 meteorological processes, *Sci. Total Environ.*, 656, 1261–1279,
490 <https://doi.org/10.1016/j.scitotenv.2018.11.366>, 2019.
- 491 Bond, T. C., Doherty, S. J., Fahey, D. W., Forster, P. M., Berntsen, T., DeAngelo, B. J.,
492 Flanner, M. G., Ghan, S., Kärcher, B., Koch, D., Kinne, S., Kondo, Y., Quinn, P.
493 K., Sarofim, M. C., Schultz, M. G., Schulz, M., Venkataraman, C., Zhang, H.,
494 Zhang, S., Bellouin, N., Guttikunda, S. K., Hopke, P. K., Jacobson, M. Z., Kaiser,
495 J. W., Klimont, Z., Lohmann, U., Schwarz, J. P., Shindell, D., Storelvmo, T.,
496 Warren, S. G., and Zender, C. S.: Bounding the role of black carbon in the climate
497 system: A scientific assessment, *J. Geophys. Res.-Atmos.*, 118, 5380–5552,
498 <https://doi.org/10.1002/jgrd.50171>, 2013.
- 499 Bond, T. C., Habib, G., and Bergstrom, R. W.: Limitations in the enhancement of visible
500 light absorption due to mixing state, *J. Geophys. Res.*, 111, D20211,
501 <https://doi.org/10.1029/2006JD007315>, 2006.
- 502 Boonpeng, B., ChooChuay, C., Dejchanchaiwong, R., Tekasakul, P., Nim, N., Bunyarit,
503 C., Choodum, A., Areerob, T., Kleangklaio, B., Wandee, S., Pianroj, Y., and Jumrat,
504 S.: An investigation of carbonaceous components and source identification of
505 ultrafine particulate matter in the atmosphere of the southern region of thailand,
506 *Aerosol Air Qual. Res.*, 26, 8, <https://doi.org/10.1007/s44408-025-00084-0>, 2026.
- 507 Cappa, C. D., Onasch, T. B., Massoli, P., Worsnop, D. R., Bates, T. S., Cross, E. S.,
508 Davidovits, P., Hakala, J., Hayden, K. L., Jobson, B. T., Kolesar, K. R., Lack, D.
509 A., Lerner, B. M., Li, S.-M., Mellon, D., Nuaaman, I., Olfert, J. S., Petäjä, T.,



- 510 Quinn, P. K., Song, C., Subramanian, R., Williams, E. J., and Zaveri, R. A.:
511 Radiative absorption enhancements due to the mixing state of atmospheric black
512 carbon, *Science*, 337, 1078–1081, <https://doi.org/10.1126/science.1223447>, 2012.
- 513 Cappa, C. D., Zhang, X., Russell, L. M., Collier, S., Lee, A. K. Y., Chen, C., Betha, R.,
514 Chen, S., Liu, J., Price, D. J., Sanchez, K. J., McMeeking, G. R., Williams, L. R.,
515 Onasch, T. B., Worsnop, D. R., Abbatt, J., and Zhang, Q.: Light absorption by
516 ambient black and brown carbon and its dependence on black carbon coating state
517 for two California, USA, cities in winter and summer, *J. Geophys. Res.-Atmos.*,
518 124, 1550–1577, <https://doi.org/10.1029/2018JD029501>, 2019.
- 519 Chen, B., Bai, Z., Cui, X., Chen, J., Andersson, A., and Gustafsson, Ö.: Light absorption
520 enhancement of black carbon from urban haze in Northern China winter, *Environ.*
521 *Pollut.*, 221, 418–426, <https://doi.org/10.1016/j.envpol.2016.12.004>, 2017.
- 522 Chen, L. W. A., Chow, J. C., Wang, X. L., Robles, J. A., Sunlin, B. J., Lowenthal, D.
523 H., Zimmermann, R., and Watson, J. G.: Multi-wavelength optical measurement
524 to enhance thermal/optical analysis for carbonaceous aerosol, *Atmos. Meas. Tech.*,
525 8, 451–461, <https://doi.org/10.5194/amt-8-451-2015>, 2015.
- 526 Chen, X., Ching, J., Wu, F., Matsui, H., Jacobson, M. Z., Zhang, F., Wang, Y., Zhang,
527 Z., Liu, D., Zhu, S., Rudich, Y., Shi, Z., Yoo, H., Jeon, K.-J., and Li, W.: Locating
528 the missing absorption enhancement due to multi-core black carbon aerosols, *Nat.*
529 *Commun.*, 16, 10187, <https://doi.org/10.1038/s41467-025-65079-2>, 2025.
- 530 Choudhary, V., Rajput, P., Rajeev, P., and Gupta, T.: Synergistic effect in absorption
531 properties of brown carbon and elemental carbon over IGP during weak southwest
532 monsoon, *Aerosol Sci. Eng.*, 1, 138–149, [https://doi.org/10.1007/s41810-017-](https://doi.org/10.1007/s41810-017-0013-1)
533 0013-1, 2017.
- 534 Chow, J. C., Watson, J. G., Chen, L.-W. A., Chang, M. C. O., Robinson, N. F., Trimble,
535 D., and Kohl, S.: The IMPROVE_A Temperature Protocol for Thermal/Optical
536 Carbon Analysis: Maintaining Consistency with a Long-Term Database, *Journal*
537 *of the Air & Waste Management Association*, 57, 1014–1023,



- 538 <https://doi.org/10.3155/1047-3289.57.9.1014>, 2007.
- 539 Chow, J. C., Watson, J. G., Green, M. C., Wang, X., Chen, L.-W. A., Trimble, D. L.,
540 Cropper, P. M., Kohl, S. D., and Gronstal, S. B.: Separation of brown carbon from
541 black carbon for IMPROVE and Chemical Speciation Network PM_{2.5} samples, *J.*
542 *Air Waste Manage.*, 68, 494–510,
543 <https://doi.org/10.1080/10962247.2018.1426653>, 2018.
- 544 Chung, S. H.: Climate response of direct radiative forcing of anthropogenic black
545 carbon, *J. Geophys. Res.*, 110, D11102, <https://doi.org/10.1029/2004JD005441>,
546 2005.
- 547 Cui, X., Wang, X., Yang, L., Chen, B., Chen, J., Andersson, A., and Gustafsson, Ö.:
548 Radiative absorption enhancement from coatings on black carbon aerosols, *Sci.*
549 *Total Environ.*, 551–552, 51–56, <https://doi.org/10.1016/j.scitotenv.2016.02.026>,
550 2016.
- 551 Curci, G., Alyuz, U., Barò, R., Bianconi, R., Bieser, J., Christensen, J. H., Colette, A.,
552 Farrow, A., Francis, X., Jiménez-Guerrero, P., Im, U., Liu, P., Manders, A.,
553 Palacios-Peña, L., Prank, M., Pozzoli, L., Sokhi, R., Solazzo, E., Tuccella, P., Unal,
554 A., Vivanco, M. G., Hogrefe, C., and Galmarini, S.: Modelling black carbon
555 absorption of solar radiation: Combining external and internal mixing assumptions,
556 *Atmos. Chem. Phys.*, 19, 181–204, <https://doi.org/10.5194/acp-19-181-2019>,
557 2019.
- 558 Dahlkötter, F., Gysel, M., Sauer, D., Minikin, A., Baumann, R., Seifert, P., Ansmann,
559 A., Fromm, M., Voigt, C., and Weinzierl, B.: The Pagami Creek smoke plume after
560 long-range transport to the upper troposphere over Europe – aerosol properties and
561 black carbon mixing state, *Atmos. Chem. Phys.*, 14, 6111–6137,
562 <https://doi.org/10.5194/acp-14-6111-2014>, 2014.
- 563 Fan, R., Ma, Y., Cao, W., Jin, S., Liu, B., Wang, W., Li, H., and Gong, W.: New insights
564 into black carbon light absorption enhancement: A comprehensive analysis of two
565 differential behaviors, *Environ. Pollut.*, 355, 124175,



- 566 <https://doi.org/10.1016/j.envpol.2024.124175>, 2024.
- 567 Fierce, L., Bond, T. C., Bauer, S. E., Mena, F., and Riemer, N.: Black carbon absorption
568 at the global scale is affected by particle-scale diversity in composition, *Nat.*
569 *Commun.*, 7, 12361, <https://doi.org/10.1038/ncomms12361>, 2016.
- 570 Flanner, M. G., Zender, C. S., Randerson, J. T., and Rasch, P. J.: Present-day climate
571 forcing and response from black carbon in snow, *J. Geophys. Res.*, 112, D11202,
572 <https://doi.org/10.1029/2006JD008003>, 2007.
- 573 Fu, X., Li, X., Zhang, F., Ren, Z., Ge, A., Zhang, X., Fang, Z., Song, W., Deng, W.,
574 Zhang, Y., Rudich, Y., and Wang, X.: Evolution of Light Absorption Enhancement
575 of Black Carbon Aerosols From Biomass Burning in Atmospheric Photochemical
576 Aging, *J. Geophys. Res.-Atmos.*, 129, e2024JD040756,
577 <https://doi.org/10.1029/2024JD040756>, 2024.
- 578 Han, Y. M., Cao, J. J., Lee, S. C., Ho, K. F., and An, Z. S.: Different characteristics of
579 char and soot in the atmosphere and their ratio as an indicator for source
580 identification in Xi'an, China, *Atmos. Chem. Phys.*, 10, 595–607,
581 <https://doi.org/10.5194/acp-10-595-2010>, 2010.
- 582 Han, Y. M., Han, Z. W., Cao, J. J., Chow, J. C., Watson, J. G., An, Z. S., Liu, S. X., and
583 Zhang, R. J.: Distribution and origin of carbonaceous aerosol over a rural high-
584 mountain lake area, Northern China and its transport significance, *Atmos. Environ.*,
585 42, 2405–2414, <https://doi.org/10.1016/j.atmosenv.2007.12.020>, 2008.
- 586 Jacobson, M. Z.: Strong radiative heating due to the mixing state of black carbon in
587 atmospheric aerosols, *Nature*, 409, 695–697, <https://doi.org/10.1038/35055518>,
588 2001.
- 589 Jin, Y., Wang, J., Liu, C., Wong, D. C., Sarwar, G., Fahey, K. M., Wu, S., Wang, J., Cai,
590 J., Tian, Z., Zhang, Z., Xing, J., Ding, A., and Wang, S.: Accounting for the black
591 carbon aging process in a two-way coupled meteorology–air quality model, *Atmos.*
592 *Chem. Phys.*, 25, 2613–2630, <https://doi.org/10.5194/acp-25-2613-2025>, 2025.
- 593 Kaskaoutis, D. G., Grivas, G., Stavroulas, I., Bougiatioti, A., Liakakou, E., Dumka, U.



594 C., Gerasopoulos, E., and Mihalopoulos, N.: Apportionment of black and brown
595 carbon spectral absorption sources in the urban environment of Athens, Greece,
596 during winter, *Sci. Total Environ.*, 801, 149739,
597 <https://doi.org/10.1016/j.scitotenv.2021.149739>, 2021.

598 Kelesidis, G. A., Neubauer, D., Fan, L.-S., Lohmann, U., and Pratsinis, S. E.: Enhanced
599 light absorption and radiative forcing by black carbon agglomerates, *Environ. Sci.*
600 *Technol.*, 56, 8610–8618, <https://doi.org/10.1021/acs.est.2c00428>, 2022.

601 Kong, Y., Zhi, G., Jin, W., Zhang, Y., Shen, Y., Li, Z., Sun, J., and Ren, Y.: A review of
602 quantification methods for light absorption enhancement of black carbon aerosol,
603 *Sci. Total Environ.*, 924, 171539, <https://doi.org/10.1016/j.scitotenv.2024.171539>,
604 2024.

605 Lack, D. A. and Cappa, C. D.: Impact of brown and clear carbon on light absorption
606 enhancement, single scatter albedo and absorption wavelength dependence of
607 black carbon, *Atmos. Chem. Phys.*, 10, 4207–4220, [https://doi.org/10.5194/acp-](https://doi.org/10.5194/acp-10-4207-2010)
608 [10-4207-2010](https://doi.org/10.5194/acp-10-4207-2010), 2010.

609 Lack, D. A. and Langridge, J. M.: On the attribution of black and brown carbon light
610 absorption using the Ångström exponent, *Atmos. Chem. Phys.*, 13, 10535–10543,
611 <https://doi.org/10.5194/acp-13-10535-2013>, 2013.

612 Lack, D. A., Langridge, J. M., Bahreini, R., Cappa, C. D., Middlebrook, A. M., and
613 Schwarz, J. P.: Brown carbon and internal mixing in biomass burning particles, *P.*
614 *Natl. Acad. Sci. USA*, 109, 14802–14807,
615 <https://doi.org/10.1073/pnas.1206575109>, 2012.

616 Laskin, A., Laskin, J., and Nizkorodov, S. A.: Chemistry of atmospheric brown carbon,
617 *Chem. Rev.*, 115, 4335–4382, <https://doi.org/10.1021/cr5006167>, 2015.

618 Laskin, A., West, C. P., and Hettiyadura, A. P. S.: Molecular insights into the
619 composition, sources, and aging of atmospheric brown carbon, *Chem. Soc. Rev.*,
620 54, 1583–1612, <https://doi.org/10.1039/D3CS00609C>, 2025.

621 Li, H. Z., Dallmann, T. R., Li, X., Gu, P., and Presto, A. A.: Urban organic aerosol



- 622 exposure: Spatial variations in composition and source impacts, *Environ. Sci.*
623 *Technol.*, 52, 415–426, <https://doi.org/10.1021/acs.est.7b03674>, 2018.
- 624 Li, J., Liu, C., Yin, Y., and Kumar, K. R.: Numerical investigation on the ångström
625 exponent of black carbon aerosol, *J. Geophys. Res.-Atmos.*, 121, 3506–3518,
626 <https://doi.org/10.1002/2015JD024718>, 2016.
- 627 Li, S., Zhang, H., Wang, Z., and Chen, Y.: Advances in the research on brown carbon
628 aerosols: Its concentrations, radiative forcing, and effects on climate, *Aerosol Air*
629 *Qual. Res.*, 23, 220336, <https://doi.org/10.4209/aaqr.220336>, 2023a.
- 630 Li, Z., Zhi, G., Zhang, Y., Jin, W., Sun, J., Kong, Y., Shen, Y., and Zhang, H.: The
631 integrating sphere system plus in-situ absorption monitoring: A new scheme to
632 study absorption enhancement of black carbon in ambient aerosols, *Sci. Total*
633 *Environ.*, 892, 164355, <https://doi.org/10.1016/j.scitotenv.2023.164355>, 2023b.
- 634 Liu, B., Zhang, J., Wang, L., Liang, D., Cheng, Y., Wu, J., Bi, X., Feng, Y., Zhang, Y.,
635 and Yang, H.: Characteristics and sources of the fine carbonaceous aerosols in
636 Haikou, China, *Atmos. Res.*, 199, 103–112,
637 <https://doi.org/10.1016/j.atmosres.2017.08.022>, 2018a.
- 638 Liu, C., Chung, C. E., Yin, Y., and Schnaiter, M.: The absorption ångström exponent of
639 black carbon: from numerical aspects, *Atmos. Chem. Phys.*, 18, 6259–6273,
640 <https://doi.org/10.5194/acp-18-6259-2018>, 2018b.
- 641 Liu, J., Christensen, J. H., Ye, Z., Dong, S., Geels, C., Brandt, J., Nenes, A., Yuan, Y.,
642 and Im, U.: Impact of meteorology and aerosol sources on PM_{2.5} and oxidative
643 potential variability and levels in China, *Atmos. Chem. Phys.*, 24, 10849–10867,
644 <https://doi.org/10.5194/acp-24-10849-2024>, 2024.
- 645 Liu, S., Aiken, A. C., Gorkowski, K., Dubey, M. K., Cappa, C. D., Williams, L. R.,
646 Herndon, S. C., Massoli, P., Fortner, E. C., Chhabra, P. S., Brooks, W. A., Onasch,
647 T. B., Jayne, J. T., Worsnop, D. R., China, S., Sharma, N., Mazzoleni, C., Xu, L.,
648 Ng, N. L., Liu, D., Allan, J. D., Lee, J. D., Fleming, Z. L., Mohr, C., Zotter, P.,
649 Szidat, S., and Prévôt, A. S. H.: Enhanced light absorption by mixed source black



- 650 and brown carbon particles in UK winter, *Nat. Commun.*, 6, 8435,
651 <https://doi.org/10.1038/ncomms9435>, 2015.
- 652 Luo, J., Zhang, Y., and Zhang, Q.: Effects of black carbon morphology on brown carbon
653 absorption estimation: From numerical aspects, *Geosci. Model Dev.*, 14, 2113–
654 2126, <https://doi.org/10.5194/gmd-14-2113-2021>, 2021.
- 655 Luo, J., Zhang, Y., Wang, F., and Zhang, Q.: Effects of brown coatings on the absorption
656 enhancement of black carbon: a numerical investigation, *Atmos. Chem. Phys.*, 18,
657 16897–16914, <https://doi.org/10.5194/acp-18-16897-2018>, 2018.
- 658 Mbengue, S., Zikova, N., Schwarz, J., Vodička, P., Šmejkalová, A. H., and Holoubek,
659 I.: Mass absorption cross-section and absorption enhancement from long term
660 black and elemental carbon measurements: A rural background station in central
661 Europe, *Sci. Total Environ.*, 794, 148365,
662 <https://doi.org/10.1016/j.scitotenv.2021.148365>, 2021.
- 663 Moschos, V., Gysel-Beer, M., Modini, R. L., Corbin, J. C., Massabò, D., Costa, C.,
664 Danelli, S. G., Vlachou, A., Daellenbach, K. R., Szidat, S., Prati, P., Prévôt, A. S.
665 H., Baltensperger, U., and El Haddad, I.: Source-specific light absorption by
666 carbonaceous components in the complex aerosol matrix from yearly filter-based
667 measurements, *Atmos. Chem. Phys.*, 21, 12809–12833,
668 <https://doi.org/10.5194/acp-21-12809-2021>, 2021.
- 669 Peng, C., Yang, F., Tian, M., Shi, G., Li, L., Huang, R.-J., Yao, X., Luo, B., Zhai, C.,
670 and Chen, Y.: Brown carbon aerosol in two megacities in the Sichuan Basin of
671 southwestern China: Light absorption properties and implications, *Sci. Total*
672 *Environ.*, 719, 137483, <https://doi.org/10.1016/j.scitotenv.2020.137483>, 2020.
- 673 Peng, J., Hu, M., Shang, D., Wu, Z., Du, Z., Tan, T., Wang, Y., Zhang, F., and Zhang,
674 R.: Explosive secondary aerosol formation during severe haze in the North China
675 Plain, *Environ. Sci. Technol.*, 55, 2189–2207,
676 <https://doi.org/10.1021/acs.est.0c07204>, 2021.
- 677 Penner, J. E., Chuang, C. C., and Grant, K.: Climate forcing by carbonaceous and sulfate



- 678 aerosols, *Clim. Dynam.*, 14, 839–851, <https://doi.org/10.1007/s003820050259>,
679 1998.
- 680 Pokhrel, R. P., Beamesderfer, E. R., Wagner, N. L., Langridge, J. M., Lack, D. A.,
681 Jayarathne, T., Stone, E. A., Stockwell, C. E., Yokelson, R. J., and Murphy, S. M.:
682 Relative importance of black carbon, brown carbon, and absorption enhancement
683 from clear coatings in biomass burning emissions, *Atmos. Chem. Phys.*, 17, 5063–
684 5078, <https://doi.org/10.5194/acp-17-5063-2017>, 2017.
- 685 Ravindra, K., Singh, T., Mandal, T. K., Sharma, S. K., and Mor, S.: Seasonal variations
686 in carbonaceous species of PM_{2.5} aerosols at an urban location situated in Indo-
687 Gangetic Plain and its relationship with transport pathways, including the potential
688 sources, *J. Environ. Manage.*, 303, 114049,
689 <https://doi.org/10.1016/j.jenvman.2021.114049>, 2022.
- 690 Reisinger, P., Wonaschütz, A., Hitzenberger, R., Petzold, A., Bauer, H., Jankowski, N.,
691 Puxbaum, H., Chi, X., and Maenhaut, W.: Intercomparison of measurement
692 techniques for black or elemental carbon under urban background conditions in
693 wintertime: Influence of biomass combustion, *Environ. Sci. Technol.*, 42, 884–889,
694 <https://doi.org/10.1021/es0715041>, 2008.
- 695 Samset, B. H., Wilcox, L. J., Allen, R. J., Stjern, C. W., Lund, M. T., Ahmadi, S., Ekman,
696 A., Elling, M. T., Fraser-Leach, L., Griffiths, P., Keeble, J., Koshiro, T., Kushner,
697 P., Lewinschal, A., Makkonen, R., Merikanto, J., Nabat, P., Narazenko, L.,
698 O'Donnell, D., Oshima, N., Rumbold, S. T., Takemura, T., Tsigaridis, K., and
699 Westervelt, D. M.: East asian aerosol cleanup has likely contributed to the recent
700 acceleration in global warming, *Commun Earth Environ*, 6, 543,
701 <https://doi.org/10.1038/s43247-025-02527-3>, 2025.
- 702 Schnaiter, M.: Absorption amplification of black carbon internally mixed with
703 secondary organic aerosol, *J. Geophys. Res.*, 110, D19204,
704 <https://doi.org/10.1029/2005JD006046>, 2005.
- 705 Schwarz, J. P., Spackman, J. R., Fahey, D. W., Gao, R. S., Lohmann, U., Stier, P., Watts,



- 706 L. A., Thomson, D. S., Lack, D. A., Pfister, L., Mahoney, M. J., Baumgardner, D.,
707 Wilson, J. C., and Reeves, J. M.: Coatings and their enhancement of black carbon
708 light absorption in the tropical atmosphere, *J. Geophys. Res.*, 113, D03203,
709 <https://doi.org/10.1029/2007JD009042>, 2008.
- 710 Selimovic, V., Yokelson, R. J., McMeeking, G. R., and Coefield, S.: In situ
711 measurements of trace gases, PM, and aerosol optical properties during the 2017
712 NW US wildfire smoke event, *Atmos. Chem. Phys.*, 19, 3905–3926,
713 <https://doi.org/10.5194/acp-19-3905-2019>, 2019.
- 714 Shen, Y., Zhi, G., Jin, W., Kong, Y., Zhang, Y., Li, Z., Sun, J., Wang, Y., and Liang, Z.:
715 Beijing air quality and light absorption coefficients dataset 2023 [data set],
716 <https://doi.org/10.5281/zenodo.18552344>, 2026.
- 717 Shiraiwa, M., Kondo, Y., Iwamoto, T., and Kita, K.: Amplification of light absorption
718 of black carbon by organic coating, *Aerosol Sci. Tech.*, 44, 46–54,
719 <https://doi.org/10.1080/02786820903357686>, 2010.
- 720 Song, J., Saathoff, H., Gao, L., Gebhardt, R., Jiang, F., Vallon, M., Bauer, J., Norra, S.,
721 and Leisner, T.: Variations of PM_{2.5} sources in the context of meteorology and
722 seasonality at an urban street canyon in southwest Germany, *Atmos. Environ.*, 282,
723 119147, <https://doi.org/10.1016/j.atmosenv.2022.119147>, 2022.
- 724 Sun, J., Zhang, Y., Zhi, G., Hitzenberger, R., Jin, W., Chen, Y., Wang, L., Tian, C., Li,
725 Z., Chen, R., Xiao, W., Cheng, Y., Yang, W., Yao, L., Cao, Y., Huang, D., Qiu, Y.,
726 Xu, J., Xia, X., Yang, X., Zhang, X., Zong, Z., Song, Y., and Wu, C.: Brown
727 carbon’s emission factors and optical characteristics in household biomass burning:
728 developing a novel algorithm for estimating the contribution of brown carbon,
729 *Atmos. Chem. Phys.*, 21, 2329–2341, <https://doi.org/10.5194/acp-21-2329-2021>,
730 2021.
- 731 Sun, J., Zhi, G., Hitzenberger, R., Chen, Y., Tian, C., Zhang, Y., Feng, Y., Cheng, M.,
732 Zhang, Y., Cai, J., Chen, F., Qiu, Y., Jiang, Z., Li, J., Zhang, G., and Mo, Y.:
733 Emission factors and light absorption properties of brown carbon from household



- 734 coal combustion in China, *Atmos. Chem. Phys.*, 17, 4769–4780,
735 <https://doi.org/10.5194/acp-17-4769-2017>, 2017.
- 736 Thuillier, G., Hersé, M., Labs, D., Foujols, T., Peetermans, W., Gillotay, D., Simon, P.
737 C., and Mandel, H.: The Solar Spectral Irradiance from 200 to 2400 nm as
738 Measured by the SOLSPEC Spectrometer from the Atlas and Eureka Missions, *Sol.*
739 *Phys.*, 214, 1–22, <https://doi.org/10.1023/A:1024048429145>, 2003.
- 740 Tohidi, R., Altuwayjiri, A., and Sioutas, C.: Investigation of organic carbon profiles and
741 sources of coarse PM in los angeles, *Environmental Pollution*, 314, 120264,
742 <https://doi.org/10.1016/j.envpol.2022.120264>, 2022.
- 743 Wang, L., Jin, W., Sun, J., Zhi, G., Li, Z., Zhang, Y., Guo, S., He, J., and Zhao, C.:
744 Seasonal features of brown carbon in northern China: Implications for BrC
745 emission control, *Atmos. Res.*, 257, 105610,
746 <https://doi.org/10.1016/j.atmosres.2021.105610>, 2021a.
- 747 Wang, Q., Han, Y., Ye, J., Liu, S., Pongpiachan, S., Zhang, N., Han, Y., Tian, J., Wu, C.,
748 Long, X., Zhang, Q., Zhang, W., Zhao, Z., and Cao, J.: High contribution of
749 secondary brown carbon to aerosol light absorption in the southeastern margin of
750 Tibetan Plateau, *Geophys. Res. Lett.*, 46, 4962–4970,
751 <https://doi.org/10.1029/2019GL082731>, 2019a.
- 752 Wang, Q., Jacob, D. J., Spackman, J. R., Perring, A. E., Schwarz, J. P., Moteki, N.,
753 Marais, E. A., Ge, C., Wang, J., and Barrett, S. R. H.: Global budget and radiative
754 forcing of black carbon aerosol: Constraints from pole-to-pole (HIPPO)
755 observations across the Pacific, *J. Geophys. Res.-Atmos.*, 119, 195–206,
756 <https://doi.org/10.1002/2013JD020824>, 2014.
- 757 Wang, Q., Liu, H., Ye, J., Tian, J., Zhang, T., Zhang, Y., Liu, S., and Cao, J.: Estimating
758 absorption Ångström exponent of black carbon aerosol by coupling
759 multiwavelength absorption with chemical composition, *Environ. Sci. Technol.*
760 *Lett.*, 8, 121–127, <https://doi.org/10.1021/acs.estlett.0c00829>, 2021b.
- 761 Wang, Q., Ye, J., Wang, Y., Zhang, T., Ran, W., Wu, Y., Tian, J., Li, L., Zhou, Y., Ho, S.



- 762 S. H., Dang, B., Zhang, Q., Zhang, R., Chen, Y., Zhu, C., and Cao, J.: Wintertime
763 optical properties of primary and secondary brown carbon at a regional site in the
764 North China Plain, *Environ. Sci. Technol.*, 53, 12389–12397,
765 <https://doi.org/10.1021/acs.est.9b03406>, 2019b.
- 766 Wang, X., Heald, C. L., Liu, J., Weber, R. J., Campuzano-Jost, P., Jimenez, J. L.,
767 Schwarz, J. P., and Perring, A. E.: Exploring the observational constraints on the
768 simulation of brown carbon, *Atmos. Chem. Phys.*, 18, 635–653,
769 <https://doi.org/10.5194/acp-18-635-2018>, 2018.
- 770 Wonaschütz, A., Hitznerberger, R., Bauer, H., Pouresmaeil, P., Klatzer, B., Caseiro, A.,
771 and Puxbaum, H.: Application of the integrating sphere method to separate the
772 contributions of brown and black carbon in atmospheric aerosols, *Environ. Sci.*
773 *Technol.*, 43, 1141–1146, <https://doi.org/10.1021/es8008503>, 2009.
- 774 Wu, G., Ram, K., Fu, P., Wang, W., Zhang, Y., Liu, X., Stone, E. A., Pradhan, B. B.,
775 Dangol, P. M., Panday, A. K., Wan, X., Bai, Z., Kang, S., Zhang, Q., and Cong, Z.:
776 Water-soluble brown carbon in atmospheric aerosols from Godavari (Nepal), a
777 regional representative of South Asia, *Environ. Sci. Technol.*, 53, 3471–3479,
778 <https://doi.org/10.1021/acs.est.9b00596>, 2019.
- 779 Wu, G.-M., Cong, Z.-Y., Kang, S.-C., Kawamura, K., Fu, P.-Q., Zhang, Y.-L., Wan, X.,
780 Gao, S.-P., and Liu, B.: Brown carbon in the cryosphere: Current knowledge and
781 perspective, *Adv. Clim. Change Res.*, 7, 82–89,
782 <https://doi.org/10.1016/j.accre.2016.06.002>, 2016a.
- 783 Wu, Y., Zhang, R., Tian, P., Tao, J., Hsu, S.-C., Yan, P., Wang, Q., Cao, J., Zhang, X.,
784 and Xia, X.: Effect of ambient humidity on the light absorption amplification of
785 black carbon in Beijing during January 2013, *Atmos. Environ.*, 124, 217–223,
786 <https://doi.org/10.1016/j.atmosenv.2015.04.041>, 2016b.
- 787 Xie, C., Xu, W., Wang, J., Liu, D., Ge, X., Zhang, Q., Wang, Q., Du, W., Zhao, J., Zhou,
788 W., Li, J., Fu, P., Wang, Z., Worsnop, D., and Sun, Y.: Light absorption
789 enhancement of black carbon in urban Beijing in summer, *Atmos. Environ.*, 213,



- 790 499–504, <https://doi.org/10.1016/j.atmosenv.2019.06.041>, 2019.
- 791 Xie, Y., Zeng, L., Hu, S., Wang, T., Du, Z., Tan, T., Xu, N., Chen, S., Mao, J., Xu, F.,
792 and Hu, M.: Long-term trends of black carbon levels, sources, and radiative effects
793 from 2013 to 2022 in Beijing, China, *npj Clim. Atmos. Sci.*, 1, 10,
794 <https://doi.org/10.1038/s44407-025-00010-z>, 2025.
- 795 Xu, X., Zhao, W., Zhang, Q., Wang, S., Fang, B., Chen, W., Venables, D. S., Wang, X.,
796 Pu, W., Wang, X., Gao, X., and Zhang, W.: Optical properties of atmospheric fine
797 particles near Beijing during the HOPE-J³A campaign, *Atmos. Chem. Phys.*, 16,
798 6421–6439, <https://doi.org/10.5194/acp-16-6421-2016>, 2016.
- 799 Yang, S., Liu, Y., Chen, L., Cao, N., Wang, J., and Gao, S.: Direct radiative forcing of
800 light-absorbing carbonaceous aerosol and the influencing factors over China,
801 *Atmos. Chem. Phys.*, 25, 9335–9355, <https://doi.org/10.5194/acp-25-9335-2025>,
802 2025.
- 803 Yue, S., Bikkina, S., Gao, M., Barrie, L. A., Kawamura, K., and Fu, P.: Sources and
804 radiative absorption of water-soluble brown carbon in the high Arctic atmosphere,
805 *Geophys. Res. Lett.*, 46, 14881–14891, <https://doi.org/10.1029/2019GL085318>,
806 2019.
- 807 Yus-Díez, J., Via, M., Alastuey, A., Karanasiou, A., Minguillón, M. C., Perez, N.,
808 Querol, X., Reche, C., Ivančič, M., Rigler, M., and Pandolfi, M.: Absorption
809 enhancement of black carbon particles in a Mediterranean city and countryside:
810 Effect of particulate matter chemistry, ageing and trend analysis, *Atmos. Chem.*
811 *Phys.*, 22, 8439–8456, <https://doi.org/10.5194/acp-22-8439-2022>, 2022.
- 812 Zhang, R., Khalizov, A. F., Pagels, J., Zhang, D., Xue, H., and McMurry, P. H.:
813 Variability in morphology, hygroscopicity, and optical properties of soot aerosols
814 during atmospheric processing, *P. Natl. Acad. Sci. USA*, 105, 10291–10296,
815 <https://doi.org/10.1073/pnas.0804860105>, 2008.
- 816 Zhang, X., Mao, M., Chen, H., Yin, Y., and Tang, S.: Lensing effect of black carbon
817 with brown coatings: Dominant microphysics and parameterization, *J. Geophys.*



818 Res.-Atmos., 126, e2020JD033549, <https://doi.org/10.1029/2020JD033549>, 2021.

819 Zhang, Y., Zhang, Q., Cheng, Y., Su, H., Kecorius, S., Wang, Z., Wu, Z., Hu, M., Zhu,
820 T., Wiedensohler, A., and He, K.: Measuring the morphology and density of
821 internally mixed black carbon with SP2 and VTDMA: new insight into the
822 absorption enhancement of black carbon in the atmosphere, *Atmos. Meas. Tech.*,
823 9, 1833–1843, <https://doi.org/10.5194/amt-9-1833-2016>, 2016.

824 Zhang, Y., Zhi, G., Jin, W., Wang, L., Guo, S., Shi, R., Sun, J., Cheng, M., Bi, F., Gao,
825 J., Zhang, B., Wu, J., Shi, Z., Liu, B., Wang, Z., and Li, S.: Differing effects of
826 escalating pollution on absorption and scattering efficiencies of aerosols: Toward
827 co-beneficial air quality enhancement and climate protection measures, *Atmos.*
828 *Environ.*, 232, 117570, <https://doi.org/10.1016/j.atmosenv.2020.117570>, 2020.

829 Zhang, Y., Zhi, G., Tian, C., Li, S., Sun, J., Zhang, Y., and Yang, T.: Study of the details
830 of aerosol carbon measurements in autumn and winter in Beijing, *Environ. Sci.*
831 *Res.*, 30, 1184–1192, <https://doi.org/10.13198/j.issn.1001-6929.2017.02.56>, 2017.

832 Zhao, G., Tan, T., Zhu, Y., Hu, M., and Zhao, C.: Method to quantify black carbon
833 aerosol light absorption enhancement with a mixing state index, *Atmos. Chem.*
834 *Phys.*, 21, 18055–18063, <https://doi.org/10.5194/acp-21-18055-2021>, 2021.

835 Zhi, G., Chen, Y., Xue, Z., Meng, F., Cai, J., Sheng, G., and Fu, J.: Comparison of
836 elemental and black carbon measurements during normal and heavy haze periods:
837 implications for research, *Environ. Monit. Assess.*, 186, 6097–6106,
838 <https://doi.org/10.1007/s10661-014-3842-2>, 2014.

839 Zhu, C., Qu, Y., Huang, H., Chen, J., Dai, W., Huang, R., and Cao, J.: Black carbon and
840 secondary brown carbon, the dominant light absorption and direct radiative forcing
841 contributors of the atmospheric aerosols over the Tibetan Plateau, *Geophys. Res.*
842 *Lett.*, 48, e2021GL092524, <https://doi.org/10.1029/2021GL092524>, 2021.

843